



Photon echo studies of rare-earth-activated materials for optical memory and signal processing devices
by Randy Wayne Equall

A thesis submitted in partial fulfillment of the requirements for the degree of Doctor of Philosophy in
Physics

Montana State University

© Copyright by Randy Wayne Equall (1995)

Abstract:

The optical spectroscopy and dynamics of three materials; $\text{Eu}^{3+}:\text{Y}_2\text{SiO}_5$, $\text{Pr}^{3+}:\text{Y}_2\text{SiO}_5$, and $\text{Tm}^{3+}:\text{Y}_2\text{SiO}_5$ that are of interest for application in persistent spectral holeburning optical memory and signal processing devices were investigated using linear and nonlinear spectroscopic techniques. Two-pulse photon echoes have been used to measure the homogeneous linewidths. The effects of instantaneous spectral diffusion were systematically studied to allow accurate determination of the optical resonance widths, and external magnetic fields were applied to characterize the effects of fluctuating nuclear spins of the host lattice on dephasing of the dopant ion.

The $7F_0 \rightarrow 5D_0$ transition of 0.1% Eu^{3+} in the two crystallographic sites of Y_2SiO_5 was studied using photon echoes. Using this material, we succeeded in measuring the narrowest optical resonance in a solid by shielding the crystal from stray electromagnetic fields and using sufficiently low laser power to minimize contributions from instantaneous diffusion. The homogeneous linewidths measured in a magnetic field of 100 G are 122 Hz (site 1) and 167 Hz (site 2). These widths are dominated by population decay, but up to 20 Hz is attributed to 89Y spin fluctuations which have been reduced by the applied magnetic field.

Similar studies were performed to determine the contributions to the homogeneous linewidth of the $3H_4(1) \rightarrow 1D_2(1)$ transition for both sites of 0.02% Pr^{3+} in Y_2SiO_5 . Linewidths of 2.1 kHz (site 1) and 0.85 kHz (site 2) were obtained with an applied magnetic field of 77 G. A significant contribution of 89Y nuclear spin fluctuations to the zero-field homogeneous linewidth was found. Optically detected nuclear magnetic resonance measurements determined the hyperfine structure of the $3H_4$ ground state for each site, and photon echo nuclear double resonance was used to determine the hyperfine levels of the lowest component of the $1D_2$ manifold.

Absorption, fluorescence, fluorescence excitation and Zeeman experiments were performed to characterize the crystal field levels of 0.1% Tm^{3+} in Y_2SiO_5 . Small splittings of only 13 cm^{-1} (site 1) and 1.6 cm^{-1} (site 2) were found for the lowest components of the $3H_6$ ground state multiplet. The homogeneous linewidth of the $3H_6 \rightarrow 3H_4$ transition was also measured yielding widths of 57 kHz (site 1) and 241 kHz (site 2) in zero magnetic field. These unexpectedly large widths were attributed to the accidental magnetic sensitivity of Tm^{3+} in this host due to the presence of enhanced nuclear magnetic moments resulting from the energy level structure.

PHOTON ECHO STUDIES OF RARE-EARTH-ACTIVATED MATERIALS
FOR OPTICAL MEMORY AND SIGNAL PROCESSING DEVICES

by

Randy Wayne Equall

A thesis submitted in partial fulfillment
of the requirements for the degree

of

Doctor of Philosophy

in

Physics

MONTANA STATE UNIVERSITY
Bozeman, Montana

May 1995

D378
Eq 25

APPROVAL

of a thesis submitted by

Randy Wayne Equall

This thesis has been read by each member of the thesis committee and has been found to be satisfactory regarding content, English usage, format, citations, bibliographic style, and consistency, and is ready for submission to the College of Graduate Studies.

5/18/95
Date

Rufus L Cone
Chairman, Graduate Committee

Approved for the Major Department

5-18-95
Date

Henn
Head, Major Department

Approved for the College of Graduate Studies

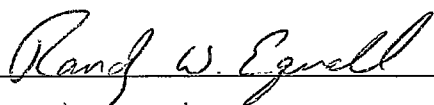
6/31/95
Date

R. Brown
Graduate Dean

STATEMENT OF PERMISSION TO USE

In presenting this thesis in partial fulfillment of the requirements for a doctoral degree at Montana State University, I agree that the Library shall make it available to borrowers under rules of the Library. I further agree that copying of this thesis is allowable only for scholarly purposes, consistent with "fair use" as prescribed in the U. S. Copyright Law. Requests for extensive copying or reproduction of this thesis should be referred to University Microfilms International, 300 North Zeeb Road, Ann Arbor, Michigan 48106, to whom I have granted "the exclusive right to reproduce and distribute my dissertation for sale in and from microform or electronic format, along with the right to reproduce and distribute my abstract in any format in whole or in part."

Signature



Date

5/18/95

ACKNOWLEDGMENTS

It is my pleasure to acknowledge the people who have helped make the work presented in this thesis possible. First and foremost, I would like to thank my advisor Rufus Cone for the opportunity to work in his lab and for his expert scientific and experimental guidance. His endless patience and encouragement have made my tenure here a truly enjoyable experience. I would also like to thank Roger Macfarlane who has been involved in all aspects of this research. Our many conversations have provided both insight and inspiration. Thanks also to Ralph Hutcheson at Scientific Materials for providing some of the crystals used in these studies.

I would also like to acknowledge my fellow students in the lab: Yongchen Sun, Guangming Wang, Meg Hall, and Greg White for their help in performing experiments and for our many useful discussions.

I also want to thank Norman Williams and Erik Andersen for their expert technical advice and aid in the construction and maintenance of the equipment that made this research possible.

Finally, I owe my wife and parents more than words can really express. Throughout my academic career they have been a constant source of support and encouragement. I especially wish to thank my wife Nancy for her patience during the many late nights when the helium just never seemed to run out.

TABLE OF CONTENTS

	Page
APPROVAL.....	ii
STATEMENT OF PERMISSION TO USE.....	iii
ACKNOWLEDGMENTS	iv
TABLE OF CONTENTS	v
LIST OF TABLES	vii
LIST OF FIGURES.....	viii
ABSTRACT.....	xii
1. INTRODUCTION.....	1
Motivation	2
Measurement Techniques	4
Materials Studies.....	5
Eu ³⁺ :Y ₂ SiO ₅	6
Pr ³⁺ :Y ₂ SiO ₅	7
Tm ³⁺ :Y ₂ SiO ₅	8
2. SPECTRAL HOLEBURNING AND PHOTON ECHOES	10
Homogeneous and Inhomogeneous Broadening	10
Spectral Holeburning.....	13
Basic Mechanisms	13
Optically Detected Nuclear Magnetic Resonance (ODNMR)	18
Application to Optical Memory Devices.....	20
Two Pulse Photon Echoes.....	22
The Density Matrix and the 2-Level System.....	23
Photon Echo Formation.....	26
Stimulated Photon Echoes.....	34
Application to Optical Memory Devices.....	36

TABLE OF CONTENTS—Continued

	Page
3. EXPERIMENTAL TECHNIQUES AND APPARATUS.....	41
Conventional Spectroscopy	42
Absorption	42
Fluorescence.....	46
Fluorescence Excitation	48
Nonlinear Spectroscopy	49
Photon Echoes.....	49
Photon Echo Nuclear Double Resonance (PENDOR)	52
ODNMR	54
4. SPECTROSCOPY AND DYNAMICS OF $\text{Eu}^{3+}:\text{Y}_2\text{SiO}_5$	56
Spectroscopy	56
Dephasing Mechanisms in Real Crystals	62
Nuclear and Electronic Spins	63
Instantaneous Diffusion	65
Photon Echo Measurements	68
Electromagnetic Shielding.....	69
Discussion	70
5. SPECTROSCOPY AND DYNAMICS OF $\text{Pr}^{3+}:\text{Y}_2\text{SiO}_5$	79
Spectroscopy	79
Photon Echo Measurements	87
6. SPECTROSCOPY AND DYNAMICS OF $\text{Tm}^{3+}:\text{Y}_2\text{SiO}_5$	96
Spectroscopy	97
Photon Echo Measurements	111
7. SUMMARY	116
REFERENCES CITED	119

LIST OF TABLES

	Page
Table 3.1 Experimental techniques and their spectral resolutions	42
Table 4.1 Hyperfine levels and spin Hamiltonian parameters for the 7F_0 ground state of Eu^{3+} in Y_2SiO_5 as measured by Yano <i>et al.</i> using ODNMR	59
Table 4.2 Hyperfine levels and spin Hamiltonian parameters for the 5D_0 excited state of Eu^{3+} in Y_2SiO_5 as measured by Yano <i>et al.</i> using holeburning.	59
Table 4.3 Spectral and relaxation parameters for the ${}^7F_0 \rightarrow {}^5D_0$ transition of 0.1% Eu^{3+} doped Y_2SiO_5	73
Table 5.1 Hyperfine levels and spin Hamiltonian parameters for the ${}^3H_4(1) \rightarrow {}^1D_2(1)$ transition for each site of Pr^{3+} in Y_2SiO_5 as measured by ODNMR and PENDOR	88
Table 5.2 Spectral and relaxation parameters for the ${}^3H_4(1)$ to ${}^1D_2(1)$ transition for each site of 0.02% $\text{Pr}^{3+}:\text{Y}_2\text{SiO}_5$	89

LIST OF FIGURES

	Page
Figure 2.1 Inhomogeneous and homogeneous linewidths shown schematically for the lowest level in a J-multiplet.....	11
Figure 2.2 The holeburning process.	14
Figure 2.3 Population reservoirs for holeburning in rare earth doped solids	16
Figure 2.4 Frequency domain PSHB optical data storage	21
Figure 2.5 The excitation pulse sequence and Bloch vector diagrams for two pulse photon echoes.....	30
Figure 2.6 Excitation pulse sequence for stimulated photon echoes.....	35
Figure 2.7 Schematic for coherent time-domain optical data storage	38
Figure 3.1 Experimental apparatus for white light absorption and laser absorption	43
Figure 3.2 Experimental apparatus for cw and pulsed fluorescence measurements	47
Figure 3.3 Experimental apparatus for two pulse and stimulated photon echoes	50
Figure 4.1 The monoclinic Y_2SiO_5 crystal structure.....	57
Figure 4.2 Energy level diagram for several of the 7F_J ground state multiplets and 5D_J excited state multiplets of Eu^{3+} for the two crystallographic sites of Y_2SiO_5 as measured by Yano <i>et. al.</i>	58

LIST OF FIGURES—Continued

	Page
Figure 4.3 Absorption coefficients versus frequency for the ${}^7F_0 \rightarrow {}^5D_0$ transition of $\text{Eu}^{3+}:\text{Y}_2\text{SiO}_5$ for both crystallographic sites.	61
Figure 4.4 The effect of instantaneous spectral diffusion on the evolution of the phases of ions participating in the echo sequence.....	66
Figure 4.5 Kilohertz PENDOR measurements on the ${}^7F_0 \rightarrow {}^5D_0$ transition (site 1) of $\text{Eu}^{3+}:\text{Y}_2\text{SiO}_5$	71
Figure 4.6 Photon echo decays on the ${}^7F_0 \rightarrow {}^5D_0$ transition of $\text{Eu}^{3+}:\text{Y}_2\text{SiO}_5$ at 1.4 K	74
Figure 4.7 Dependence of the homogeneous linewidth on excitation power density (a) for site 1 and (b) for site 2, varying both echo preparation pulses simultaneously	75
Figure 4.8 Dependence of the homogeneous linewidth on excitation power density for site 1 and site 2 measured by varying the intensity of the echo preparation pulses independently	77
Figure 5.1 Fluorescence spectra showing emission from the ${}^1D_2(1)$ level to the 3H_4 manifold recorded by exciting the ${}^3H_4(1) \rightarrow {}^1D_2(1)$ transition for each crystallographic site of 0.02% $\text{Pr}^{3+}:\text{Y}_2\text{SiO}_5$	81
Figure 5.2 Absorption spectra showing (a) the 1D_2 multiplet, and (b) the 3P_1 and 1I_6 region for both sites of 0.02% $\text{Pr}^{3+}:\text{Y}_2\text{SiO}_5$	83
Figure 5.3 Absorption coefficients versus frequency for the $\text{Pr}^{3+}:\text{Y}_2\text{SiO}_5$ ${}^3H_4(1) \rightarrow {}^1D_2(1)$ transitions for sites 1 and 2 recorded by monitoring the transmission of a single frequency cw dye laser	84

LIST OF FIGURES—Continued

	Page
Figure 5.4 Energy levels for the 3H_4 ground state multiplets and 1D_2 excited state multiplets for the two crystallographic sites of Pr^{3+} in Y_2SiO_5 at 1.4 K.....	86
Figure 5.5 Dependence of the homogeneous linewidth of the $^3H_4(1) \rightarrow ^1D_2(1)$ transition on excitation power density for site 1 and site 2 showing the contribution from instantaneous diffusion.....	90
Figure 5.6 Photon echo decays on the $^3H_4(1) \rightarrow ^1D_2(1)$ transition of $Pr^{3+}:Y_2SiO_5$ at 1.4 K. The excitation density was 0.32 W/cm^2 for site 1 and 0.26 W/cm^2 for site 2.....	91
Figure 6.1 White light absorption spectra of the 3H_4 multiplet of $0.1\% \text{ Tm}^{3+}:Y_2SiO_5$ for both crystallographic sites.....	98
Figure 6.2 White light absorption spectra for the 1G_4 multiplet of $0.1\% \text{ Tm}^{3+}$ doped Y_2SiO_5 for both crystallographic sites	99
Figure 6.3 Energy level diagram showing the important lower levels of the 3H_6 , 3H_4 , and 1G_4 multiplets for the two crystallographic sites of Tm^{3+} in Y_2SiO_5	102
Figure 6.4 Absorption coefficient versus frequency for the lowest component of the 3H_4 manifold for each site.....	103
Figure 6.5 Absorption spectra with an external magnetic field applied showing the Zeeman effect for the lowest levels of the 3H_4 multiplet for the two crystallographic sites.....	106
Figure 6.6 Absorption spectra showing the Zeeman effect for the next higher crystal field levels of the 3H_4 multiplet for both sites	107
Figure 6.7 Positions of the 3H_4 absorption peaks versus applied magnetic field showing the Zeeman effect of the ground state crystal field levels for both crystallographic sites	109

LIST OF FIGURES—Continued

	Page
Figure 6.8 Zeeman effect for the lowest 1G_4 level of site 1.....	110
Figure 6.9 Photon echo decays for the $Z_1 \rightarrow W_1$ transitions for both crystallographic sites of $Tm^{3+}:Y_2SiO_5$	112
Figure 6.10 Photon echo decay for the $Z_2 \rightarrow W_1$ transition of site 2	113

ABSTRACT

The optical spectroscopy and dynamics of three materials; $\text{Eu}^{3+}:\text{Y}_2\text{SiO}_5$, $\text{Pr}^{3+}:\text{Y}_2\text{SiO}_5$, and $\text{Tm}^{3+}:\text{Y}_2\text{SiO}_5$ that are of interest for application in persistent spectral holeburning optical memory and signal processing devices were investigated using linear and nonlinear spectroscopic techniques. Two-pulse photon echoes have been used to measure the homogeneous linewidths. The effects of instantaneous spectral diffusion were systematically studied to allow accurate determination of the optical resonance widths, and external magnetic fields were applied to characterize the effects of fluctuating nuclear spins of the host lattice on dephasing of the dopant ion.

The ${}^7\text{F}_0 \rightarrow {}^5\text{D}_0$ transition of 0.1% Eu^{3+} in the two crystallographic sites of Y_2SiO_5 was studied using photon echoes. Using this material, we succeeded in measuring the narrowest optical resonance in a solid by shielding the crystal from stray electromagnetic fields and using sufficiently low laser power to minimize contributions from instantaneous diffusion. The homogeneous linewidths measured in a magnetic field of 100 G are 122 Hz (site 1) and 167 Hz (site 2). These widths are dominated by population decay, but up to 20 Hz is attributed to ${}^{89}\text{Y}$ spin fluctuations which have been reduced by the applied magnetic field.

Similar studies were performed to determine the contributions to the homogeneous linewidth of the ${}^3\text{H}_4(1) \rightarrow {}^1\text{D}_2(1)$ transition for both sites of 0.02% Pr^{3+} in Y_2SiO_5 . Linewidths of 2.1 kHz (site 1) and 0.85 kHz (site 2) were obtained with an applied magnetic field of 77 G. A significant contribution of ${}^{89}\text{Y}$ nuclear spin fluctuations to the zero-field homogeneous linewidth was found. Optically detected nuclear magnetic resonance measurements determined the hyperfine structure of the ${}^3\text{H}_4$ ground state for each site, and photon echo nuclear double resonance was used to determine the hyperfine levels of the lowest component of the ${}^1\text{D}_2$ manifold.

Absorption, fluorescence, fluorescence excitation and Zeeman experiments were performed to characterize the crystal field levels of 0.1% Tm^{3+} in Y_2SiO_5 . Small splittings of only 13 cm^{-1} (site 1) and 1.6 cm^{-1} (site 2) were found for the lowest components of the ${}^3\text{H}_6$ ground state multiplet. The homogeneous linewidth of the ${}^3\text{H}_6 \rightarrow {}^3\text{H}_4$ transition was also measured yielding widths of 57 kHz (site 1) and 241 kHz (site 2) in zero magnetic field. These unexpectedly large widths were attributed to the accidental magnetic sensitivity of Tm^{3+} in this host due to the presence of enhanced nuclear magnetic moments resulting from the energy level structure.

CHAPTER 1

INTRODUCTION

The lanthanides, more commonly called the rare earths ($Z = 57 - 71$), lie between Barium and Hafnium in the periodic table. Insulators containing rare earth ions comprise a unique and extremely important class of solid state materials. The triply-ionized rare earths have an unfilled 4f electron shell that is shielded by outer filled $5s^2$ and $5p^6$ electron shells. In free space, the electronic structure of the 4f electrons is characterized by $2J+1$ -fold degenerate J-multiplets, with spacings resulting from the coulomb repulsion and spin-orbit interactions. In a solid, the "crystal field" acts only as a moderate perturbation on these multiplets because of the screening by the outer filled $5s^2p^6$ shells. The electronic structure of the rare earths in a solid can thus be treated as that of a free ion perturbed by a local crystal field specific to a given host material. As a result, rare earth ions in virtually any solid exhibit extremely sharp optical spectra originating from f to f electron transitions between crystal field levels of the $4f^n$ configuration. These properties make rare-earth-doped insulators ideal candidates for a wide variety of spectroscopic studies and applications. The clear and unambiguous nature of the spectra from rare earth activated solids allows for interpretation that provides insight not only into the material being studied, but also into the general area of solid state physics.

Motivation

The same properties that make rare earth doped solids interesting for fundamental scientific research also make them extremely valuable for application in a wide variety of commercial devices including solid state laser systems and optical fiber amplifiers. Recently, rare earth doped crystals have been shown to be of interest for application in new optical memory and signal processing devices based on persistent spectral hole burning (PSHB) and coherent transient phenomena.¹⁻¹¹ Such devices have the potential to dramatically increase optical storage densities and provide extremely high speed data access.¹⁻¹¹ In signal processing applications, these devices allow for processing of amplitude-, phase-, and frequency-modulated signals at GHz data rates.¹¹

In rare-earth-doped crystals, the spectral width of a transition is due to several interactions that can be classified into two major categories: homogeneous and inhomogeneous broadening. Homogeneous broadening is due to dynamic perturbations on the transition frequency due for example to phonons or fluctuating nuclear and electronic spins of the host lattice. Inhomogeneous broadening results from variations in the local environments of the dopant ions and can arise from static lattice strains and crystal defects. For rare earth crystals at low temperature, the spectral width of the lowest level of a J-multiplet is usually dominated by inhomogeneous broadening with a width of a several GHz and a homogeneous linewidth that can be several orders of magnitude smaller. These differences in the linewidths can be exploited for use in optical memories. In frequency domain PSHB memory applications, data is stored as

“structure” in a normally smooth inhomogeneously broadened absorption lineshape. This is accomplished by “burning holes” in the absorption profile by exposing the crystal to a narrow bandwidth laser that is resonant with some portion of the inhomogeneous line. This process selectively bleaches the absorption at the laser frequency by depleting the ground state population of ions resonant with the laser creating a “hole” in the inhomogeneously broadened line that is one bit of information. The width of these holes is limited by the homogeneous linewidth, and therefore the limit on the number of holes or bits which can be stored within the inhomogeneous profile is in principle determined by the ratio of the inhomogeneous to homogeneous linewidths Γ_{inh}/Γ_h . Thus a narrow homogeneous linewidth is important to obtain high storage densities.

In the time domain, information is stored in the form of optical pulse trains using stimulated photon echoes. The length of the pulse trains is limited by the homogeneous dephasing time, or coherence time, T_2 . Thus from the time domain point of view, long coherence times allow the storage of information in the form of long optical pulse trains within the coherence time of the material system^{2,3}. Long dephasing times in the time domain are exactly the same as narrow homogeneous linewidths in the frequency domain since $T_2 = 1/(\pi\Gamma_h)$. It is clear that the performance limits of such PSHB devices are material dependent. As a result, it is important to perform extensive material studies in order to characterize the potential of a given rare earth doped crystal for use in such applications. This thesis presents studies of three materials: $\text{Eu}^{3+}:\text{Y}_2\text{SiO}_5$, $\text{Pr}^{3+}:\text{Y}_2\text{SiO}_5$, and $\text{Tm}^{3+}:\text{Y}_2\text{SiO}_5$, that have recently been shown^{4,6-9} to have potential for application in

PSHB memory and signal processing devices. The fundamental material properties which determine the ultimate performance limits of the material have been explored using a variety of linear and non-linear spectroscopic techniques.

In addition to applications in optical memories, sharp optical resonances (or long coherence times) are important in that they provide very sensitive probes of small interactions or external perturbations such as superhyperfine coupling^{12,13}, tunneling splittings¹⁴, nuclear Zeeman effects¹⁵, or Stark coefficients involving fields as small as mV/cm.¹⁶

Measurement Techniques

The measurement of sub-kHz wide optical resonances in the frequency domain puts very stringent requirements on laser frequency stability and has not yet been achieved directly in a solid state system, although it has been demonstrated in gases, or rather in trapped single ions.¹⁷ The use of photon echoes in the time domain overcomes this need for stability, since the Fourier width of the excitation pulses can be chosen to be greater than the laser frequency jitter and this prepares a relatively broad packet in the inhomogeneous line; the second pulse of the echo sequence removes the inhomogeneous contribution to the linewidth.¹⁸ On the other hand, for spectral hole burning or optical free induction decay it is necessary to prepare a very sharp packet, less than the homogeneous linewidth. One drawback with the photon echo technique is the possibility of exciting echo modulation due to coherent preparation of three or more levels.¹⁹ In

cases where small splittings fall within the bandwidth of the excitation pulses, even a weak modulation can seriously distort the echo decays. Chapter 2 provides a more detailed description of the concepts of hole burning and related techniques and the theory of coherent transients and their application in optical memories. Chapter 3 describes the experimental apparatus used for the measurement of photon echoes and for the other spectroscopic techniques used in the studies presented in this thesis.

Materials Studies

The optical dephasing time of isolated ions in solids can become very long at low temperatures²⁰. At temperatures below about 2 K, dephasing times of optical transitions from the ground state to metastable levels in rare-earth doped crystals are usually limited by nuclear spin fluctuations. In the search for long coherence times, host materials have been chosen whose constituent ions have zero nuclear spin such as oxygen, low isotopic abundance of nuclear spins such as Si, or small magnetic moments such as yttrium. In this way and using long-lived metastable optical levels, subkilohertz wide optical resonances have been observed in $\text{Eu}^{3+}:\text{Y}_2\text{O}_3$ ^{21,22}, $\text{Eu}^{3+}:\text{Y}_2\text{SiO}_5$ ²³, and $\text{Eu}^{3+}:\text{YAlO}_3$ ^{24,25} and resonances only several kHz wide in others such as $\text{Pr}^{3+}:\text{YAlO}_3$ ^{18,26}, $\text{Pr}^{3+}:\text{YAG}$ ²⁷, and $\text{Cr}^{3+}:\text{Al}_2\text{O}_3$ ²⁸. We recently reported the measurement of a 122 Hz wide optical resonance in $\text{Eu}^{3+}:\text{Y}_2\text{SiO}_5$ - the narrowest yet observed in a solid and limited only by the population decay time T_1 .²⁹

Eu³⁺:Y₂SiO₅

The Y₂SiO₅ host is an ideal one in many ways, as nuclear spins have been minimized and large crystals of good optical quality can be produced, primarily as a result of the demand for its use as a laser material.³⁰⁻³² Chapter 4 presents studies of Eu³⁺:Y₂SiO₅ where we have used photon echoes to measure what we believe to be the longest dephasing time (i.e., the sharpest optical resonance) yet reported in a solid: T₂ = 2.6 ms for Eu³⁺ ions in Y₂SiO₅ at 1.4 K. This corresponds to an optical resonance width of 122 Hz (or a resonant Q ≥ 4 × 10¹²). Most of the more than 8 orders of magnitude between this value and that of the room temperature width (~ 60 GHz) comes from phonon scattering and phonon absorption processes which usually become negligible below ~ 4 K for rare-earth or transition-metal ion impurity systems. The remaining sources of dephasing are population decay by radiative or nonradiative processes or dynamic local fields due either to nuclear spin fluctuations of the host lattice nuclei, in the present case ⁸⁹Y, or to the presence of other excited ions (so-called "instantaneous diffusion").

The ⁷F₀ → ⁵D₀ transition of the Eu³⁺ ion is a good choice for these studies because the electronic magnetic moment is quenched in the ⁷F₀ ground state and is very small in the ⁵D₀ excited state³³, making the transition frequency insensitive to magnetic fluctuations. Further, the excited state lifetime of ~1 ms in many materials contributes only ~100 Hz to the total linewidth and allows one to study other sources of dephasing with great sensitivity. For example, most of the compounds studied contain yttrium,

because yttrium can be substituted by trivalent rare-earth ions without charge compensation and the fluctuating local fields due to the ^{89}Y nucleus are expected to be small since its magnetic moment is only $-0.14\mu_N$. By reducing other sources of line broadening, we have for the first time determined the contribution of the yttrium nucleus to optical line broadening and for the ${}^7\text{F}_0 \rightarrow {}^5\text{D}_0$ transition of Eu^{3+} found it to be only about 100 Hz. In all the work by other groups cited above, the lifetime (T_1) limited value was not reached, although efforts to remove the effects of nuclear spin fluctuations by coherent spin decoupling^{34,35} or choice of host matrix^{18,21,23} led to substantial linewidth reductions. One of the effects which makes it difficult to achieve the T_1 limit is excitation-density-dependent instantaneous diffusion in which time varying fields produced by optical excitation of neighboring ions contribute to dephasing.^{22,36-44} As coherence times become longer, the possibility that phonon contributions may contribute ~ 100 Hz needs to be kept in mind and the sample temperature carefully monitored.

$\text{Pr}^{3+}:\text{Y}_2\text{SiO}_5$

Like the Eu^{3+} ion, Pr^{3+} is a good choice for low sensitivity to dynamic local fields since it is an even electron ion so that in crystallographic sites with lower than axial symmetry the levels are electronic singlets where the orbital angular momentum is quenched. Chapter 5 describes an investigation of optical dephasing of the Pr^{3+} ion in Y_2SiO_5 . As in the case of $\text{Eu}^{3+}:\text{Y}_2\text{SiO}_5$ ²⁹ we find two contributions to T_2 - one that is magnetic in origin, involving magnetic field-dependent ^{89}Y nuclear spin fluctuations, and another that is due to field-independent population decay. For site 2 where the Pr^{3+} ion

has the smaller enhanced nuclear moment, the magnetic contribution can be largely suppressed, giving near- T_1 -limited dephasing. For site 1, a contribution of several hundred Hz remains due to spin-induced dephasing. These results were obtained after a detailed investigation of the contribution of instantaneous diffusion. Our studies show that, as in the case of $\text{Eu}^{3+}:\text{Y}_2\text{SiO}_5$, $\text{Pr}^{3+}:\text{Y}_2\text{SiO}_5$ is a useful material for demonstrations of time-domain storage and processing and it has an advantage that Pr^{3+} ions in site 1 have an oscillator strength two orders of magnitude higher than that in the Eu^{3+} material.

$\text{Tm}^{3+}:\text{Y}_2\text{SiO}_5$

Tm^{3+} is of particular interest because it has a transition at ~ 800 nm which is accessible with commercially available diode lasers. The Eu^{3+} and Pr^{3+} ions have been the primary rare earth ions of interest for optical memory applications, since, in addition to their insensitivity to the magnetic properties of the host lattice spins, they also have a nuclear spin of $5/2$ that results in hyperfine structure in the electronic singlets. The hyperfine structure provides a mechanism for persistent spectral hole burning that is necessary for memory applications. For signal processing applications, however, only long dephasing times are necessary. The Tm^{3+} ion has a nuclear spin of $1/2$ and therefore does not have hyperfine structure or a mechanism for persistent spectral hole burning, but it is of considerable interest for signal processing applications.

Chapter 6 presents studies of Tm^{3+} doped Y_2SiO_5 . The Y_2SiO_5 host has been shown to be a nearly ideal host for achieving long dephasing times.²⁹ Previous studies of

Tm^{3+} showed that even in a host like YAG with large magnetic moments present (the aluminum magnetic moment is $-3.6 \mu_N$) the ${}^3\text{H}_6 \rightarrow {}^3\text{H}_4$ transition has a long fluorescence lifetime of $\sim 800 \mu\text{s}$ and a relatively long coherence time of $T_2 = 105 \mu\text{s}$.⁴⁵ This corresponds to a homogeneous linewidth of $\sim 3 \text{ kHz}$. Measurement of the dephasing times of Tm^{3+} in Y_2SiO_5 yielded unexpectedly short values of $T_2 \cong 5 \mu\text{s}$. Spectroscopic studies of the Tm^{3+} crystal field levels show much more complicated spectra than expected for such a low symmetry site. Small ground state crystal field splittings were found that contribute to an enhanced nuclear magnetic moment which may explain the anomalously rapid dephasing seen in the photon echo experiments. At present, Tm^{3+}YAG remains the best candidate for use in diode laser pumped signal processing devices.

CHAPTER 2

SPECTRAL HOLEBURNING AND PHOTON ECHOES

Homogeneous and Inhomogeneous Broadening

There are two main classes of line broadening, homogeneous and inhomogeneous, that give rise to the observed spectral width of optical transitions of rare earth ions in real crystals. Homogeneous broadening of a spectral line is experienced equally by all ions in the solid and is due to dynamic fluctuations in the local crystal field or magnetic environment that act as perturbations on the transition frequency of the ion of interest. For rare earth doped solids, these dynamic perturbations on the transition frequency are typically a result of phonons and fluctuations of nuclear and electronic spins of the host lattice. In contrast to homogeneous broadening due to dynamical processes, inhomogeneous broadening is due to any static perturbation that makes the local environment around one ion in the solid different from that of another ion. These variations in the local crystal field are due to static lattice stresses and strains, crystal defects, and impurities. Inhomogeneous broadening mechanisms result in a distribution of transition frequencies which reflect the various local environments in the crystal. This is shown schematically in figure 2.1 for an inhomogeneously broadened transition of width Γ_{inh} , where each homogeneously broadened packet of width Γ_h represents a given

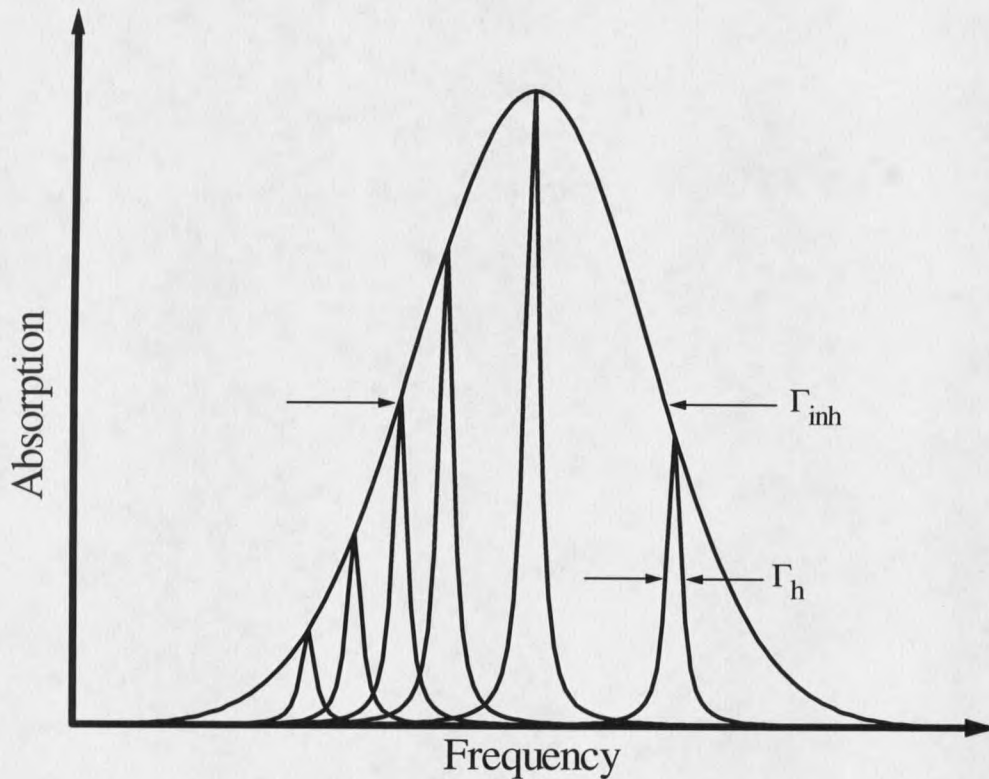


Figure 2.1 Inhomogeneous and homogeneous linewidths shown schematically for the lowest level in a J-multiplet. The homogeneous width is much smaller than the inhomogeneous width. Each homogeneously broadened “packet” represents a group of ions in the crystal that experience the same local environment.

group of ions which experience the same local environment. In rare earth doped crystals at liquid helium temperatures, the upper components of a given J-multiplet tend to have homogeneous linewidths comparable to or greater than the inhomogeneous width. This is primarily due to spontaneous phonon emission to the other lower levels in the multiplet. However, the observed spectral width of the lowest level of the multiplet is usually dominated by inhomogeneous broadening with a linewidth of a few GHz to a few

10's of GHz, and homogeneous widths of a few hundred Hz to Mhz or GHz. For studies or applications where long fluorescence lifetimes and narrow homogeneous linewidths are important, the lowest level of a manifold is typically the only state of that J-multiplet which is of interest. Since optical memory applications require these properties, the studies in this thesis were performed on transitions which are inhomogeneously broadened. While this is necessary for optical memory applications, the inhomogeneous linewidth obscures other important spectroscopic information like hyperfine or superhyperfine splittings which are on the order of kHz - MHz. The homogeneous linewidth itself contains information about the dynamics of the system and is also buried within the inhomogeneously broadened profile. Conventional spectroscopic techniques can quite easily allow for measurement of the inhomogeneous linewidth by performing a simple absorption experiment where the intensity of the transmitted light is monitored as a function of frequency. It is however a much more difficult task to determine the homogeneous linewidth, and nonlinear spectroscopic techniques must be employed to gain the extremely high resolution required to measure these structures. In the frequency domain, spectral holeburning and optically detected nuclear magnetic resonance (ODNMR) are two of the most widely used techniques, and they will be discussed in the next section. In the time domain, photon echoes and related techniques like photon echo nuclear double resonance (PENDOR) are used and are discussed in greater detail later in this chapter.

Spectral Holeburning

Basic Mechanisms

In spectral hole burning, a laser is used to selectively excite a narrow portion of the inhomogeneously broadened line. The ions which are resonant with the laser are pumped from the ground state to an excited state. These ions can then relax back to the ground state or to some other levels of the system which can act as population reservoirs. Those ions which relax back to the ground state are excited again and have another chance to decay to the other reservoir levels. In this manner, it is possible to deplete the ground state population of ions that are resonant with the laser. This selective bleaching of the absorption by the pump laser results in a spectral "hole" that may be observed by scanning the frequency of a low intensity laser across the inhomogeneously broadened line. When the low intensity laser is resonant with the original pump laser, a decrease in the absorption (increase in the transmission) is observed due to the depletion of the ground state population of ions at that frequency. This was first demonstrated in solids by Szabo in his studies of ruby,⁴⁶ and was first applied to rare earths by Erickson.⁴⁷ The holeburning process is shown schematically in figure 2.2.

The hole width and the hole lifetime are important parameters for the use of holeburning as a spectroscopic technique as well as in optical memory applications. Given a laser with a linewidth much narrower than the homogenous broadening, it is

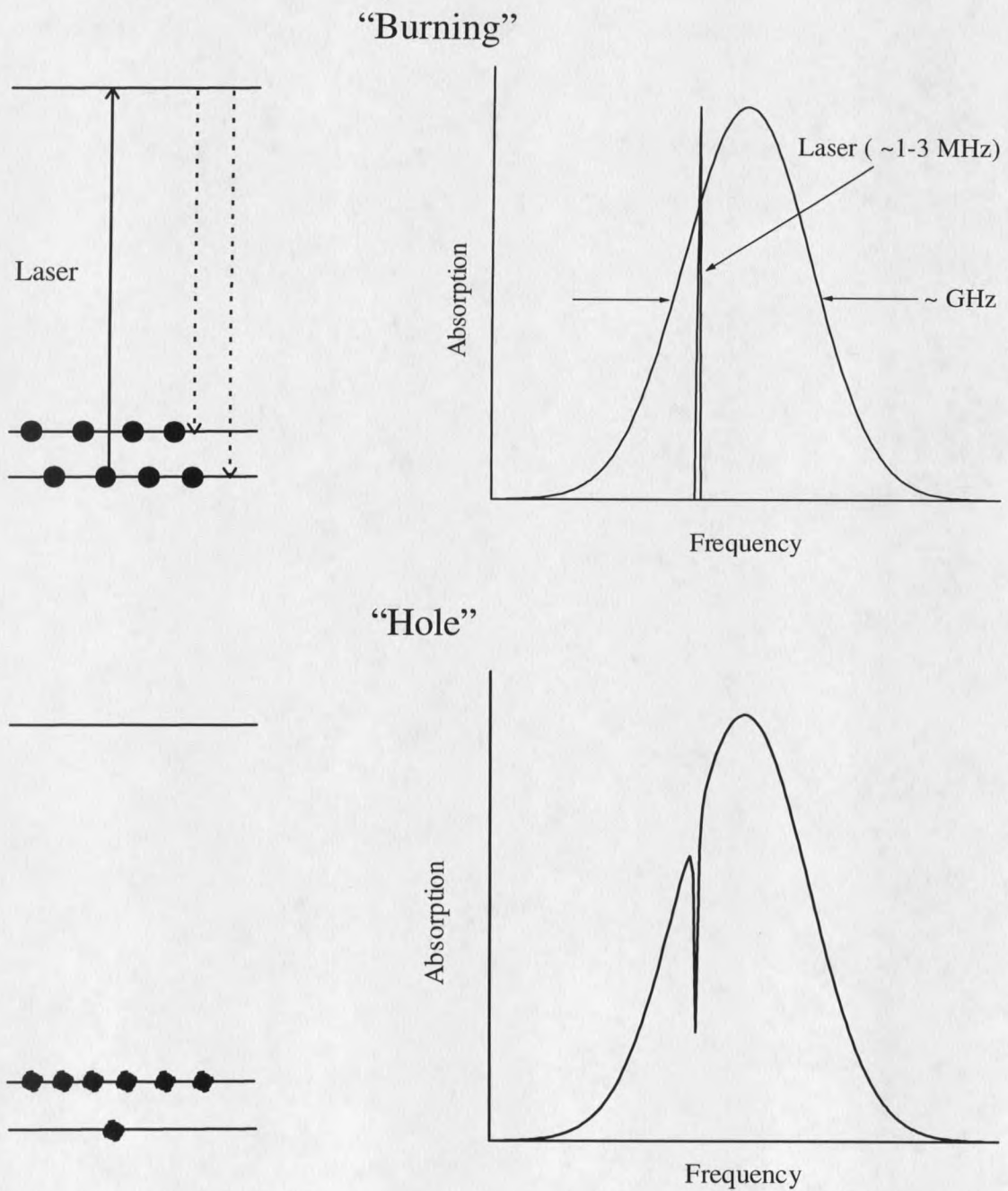
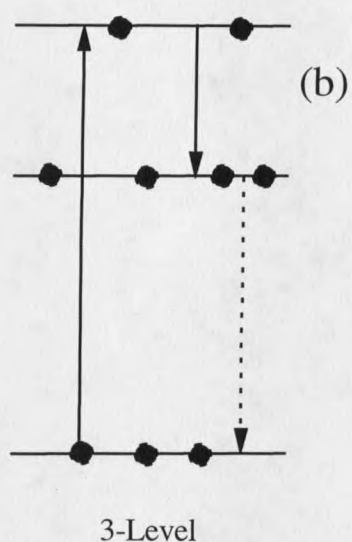
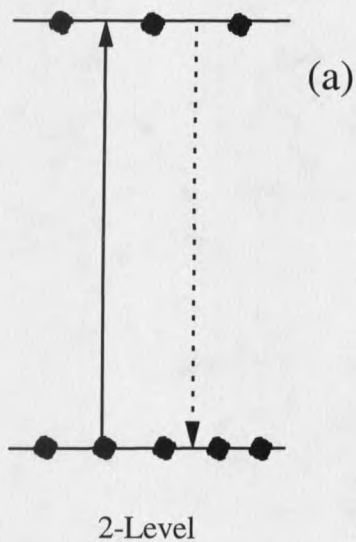


Figure 2.2 The holeburning process. A narrow band laser excites a portion of the inhomogeneous line, depleting the ground state population and enhancing the population of some other level in the system. The “Hole” can be seen as a reduction in the absorption at the frequency of the original laser.

possible to excite a single homogeneous packet, and it can be shown⁴⁸ that the hole width is twice the homogeneous linewidth plus possible power broadening effects. Commercially available single frequency cw dye lasers have jitter limited linewidths of ~ 1-3 Mhz, though, and homogeneous linewidths can be several kHz or even as narrow as a few hundred Hz. As a result, the practical resolution of the holeburning technique is determined by the stability of the laser. Much work has been done to build lasers stable to a few kHz.⁴⁹ Such lasers are not widely available though and are still too broad for use with a significant number of materials with even narrower homogeneous linewidths

The lifetime of a spectral hole is determined by the lifetime of the population reservoir and for the lowest level in a J-multiplet can range from μsec to as long as several hours in some materials.² The various mechanisms for holeburning in rare earth doped solids, shown in figure 2.3, are classified by the type of population reservoir in which the ions are stored after optical pumping from the ground state. The simplest case uses two level saturation of the absorption as the holeburning mechanism, where the excited state acts as the population reservoir. The lifetime of the hole is determined by the lifetime of the excited state, typically μsec to msec. Longer hole lifetimes can be achieved in systems where a third metastable state or hyperfine or superhyperfine structure acts as the population reservoir. Holeburning of the ${}^3\text{H}_6 \rightarrow {}^3\text{H}_4$ transition of the Tm^{3+} ion uses a three level scheme like that shown in figure 2.3b with the ${}^3\text{F}_4$ metastable level acting as the population reservoir. For Eu^{3+} and Pr^{3+} , hyperfine levels are the population reservoir as shown in figure 2.3c, and hole lifetimes of more than 13 hours have been observed.² With this potential for extremely long hole lifetimes, optical

Optical



Nuclear Spin

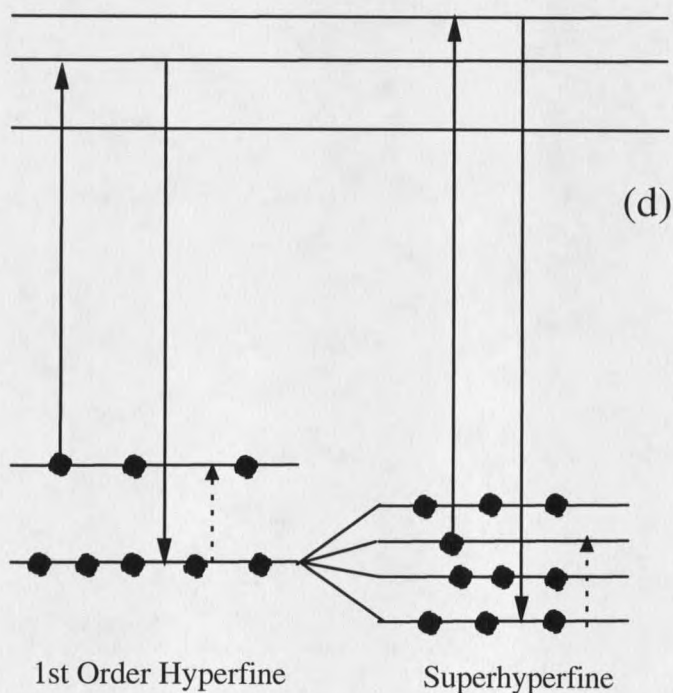
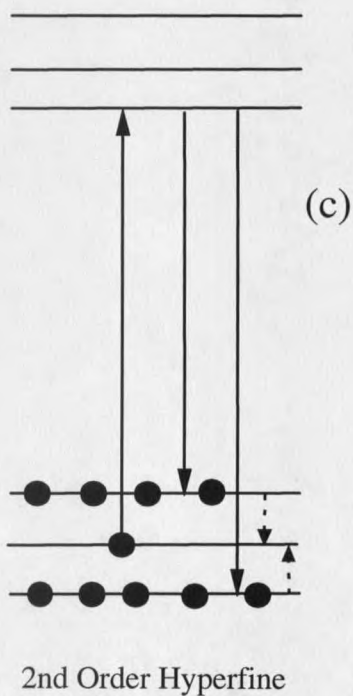


Figure 2.3 Population reservoirs for holeburning in rare earth doped solids. The solid arrows pointing up (down) show the excitation (decay) processes to (from) the excited state. The dotted arrows show the hole recovery processes that determine the lifetime of the hole.

pumping of the nuclear hyperfine levels is a very useful holeburning mechanism for the trivalent rare earths. Both Eu^{3+} and Pr^{3+} ions have a nuclear spin of $5/2$ so that in zero external magnetic field there will be three Kramers doublet nuclear hyperfine levels associated with each electronic state. In the case of Eu^{3+} , there is a significant nuclear quadrupole interaction that splits the hyperfine levels of the ${}^7\text{F}_0$ ground state and ${}^5\text{D}_0$ excited state by 10's of MHz. In Pr^{3+} the pure quadrupole interaction is quite weak but the second order magnetic hyperfine interaction or pseudo-quadrupole interaction splits the hyperfine levels of the ground state and lowest ${}^1\text{D}_2$ level on the order of 10 MHz. Holeburning is performed by using a narrow band cw laser of 1-2 MHz bandwidth to excite a single transition between the ground state and excited state hyperfine levels for one specific packet of ions in the crystal. The ground state hyperfine level which was optically pumped will have a depleted population, while the other two levels will have an excess population. If an absorption experiment is then performed, decreased absorption or holes will be seen at frequencies corresponding to transitions between the depleted level and the three excited state hyperfine levels. Enhanced absorption or antiholes will be seen at frequencies corresponding to transitions from the two ground state hyperfine levels with excess population. The relative intensities of the holes and antiholes will depend on the optical transition probability and thus on the overlap of the nuclear spin wave function of the ground and excited states. It is important to note that this pattern of holes and antiholes is for a single subset of ions in the solid. For the $\text{Eu}^{3+} {}^7\text{F}_0 \rightarrow {}^5\text{D}_0$, and $\text{Pr}^{3+} {}^3\text{H}_4 \rightarrow {}^1\text{D}_2$ transitions, the inhomogeneous broadening is very large compared to the splittings of the hyperfine levels, so all of the allowed transitions between every

